

Received December 3, 2020, accepted December 28, 2020, date of publication January 8, 2021, date of current version January 24, 2022.

Digital Object Identifier 10.1109/ACCESS.2021.3049879

# Extended State Observer-Based Nonlinear Terminal Sliding Mode Control With Feedforward Compensation for Lower Extremity Exoskeleton

YI LONG<sup>1,2</sup>, (Member, IEEE), AND YAJUN PENG<sup>3</sup>

<sup>1</sup>Foshan Graduate School, Northeastern University, Foshan 528000, China

<sup>2</sup>Faculty of Robot Science and Engineering, Northeastern University, Shenyang 110000, China

<sup>3</sup>Zhongshan Walk-Best Intelligent Medical Device Company Ltd., Zhongshan 528400, China

Corresponding author: Yi Long (longyi@mail.neu.edu.cn)

This work was supported in part by the Natural Science Foundation of Guangdong Province under Grant 2020A1515110121, and in part by the Fundamental Research Funds for the Central Universities under Grant N2129002.

**ABSTRACT** This paper presents and experimentally demonstrates an extended state observer (ESO) -based nonlinear terminal sliding mode control strategy with feedforward compensation (ESO-F-NTSMC) for lower extremity exoskeleton. Since the lower extremity exoskeleton (LEE) is a coupled human-exoskeleton coordination system, the internal or external disturbances and uncertainties affect its performance. A nonlinear terminal sliding mode control with feedforward compensation (F-NTSMC) is proposed to drive the lower extremity to shadow the target human gait trajectory. An ESO is employed to estimate the total disturbances including these caused by the chattering phenomenon in F-NTSMC. ESO-F-NTSMC can assure that the human gait trajectory tracking can converge to a bounded region smoothly and robustly. The phase identification-based human gait generation approach is also presented. The derivation process of the ESO-F-NTSMC is shown and the Lyapunov-based stability analysis is conducted. To illustrate the proposed method's effectiveness, experiments are performed on three human subjects walking on the floor at a natural speed. The results demonstrate that the exoskeleton can actively collaborate with the user under the proposed method.


**INDEX TERMS** Extended state observer, sliding mode control, gait generation, rehabilitation, exoskeleton.

## I. INTRODUCTION

Many diseases and injuries, such as stroke and spinal cord injury, have a considerable impact on these patients' normal living abilities and mental health. It is useful and necessary to develop intelligent wearable exoskeletons for rehabilitation training to regain mobility. These devices can help users practice repetitively and free physical therapists from heavy work [1]. In past decades, many kinds of wearable exoskeletons are designed to help patients rehabilitate from the jury [2]–[4]. As the exoskeleton is a typical human-machine interaction system, it is essential to design and develop control strategies to track the defined human gait safely and robustly. From the perspective of training purpose and controller design progress, the control strategies for exoskeletons can be separated into trajectory tracking control, adaptive control impedance-based control and bio-signals-based control [5]. These control strategies can also be divided into model-based and model-free methods from the perspective of model-dependence or not. The model-based techniques acquire a

full dynamics knowledge and their performance relies on the accuracy of the system model. Nevertheless, it is not easy to obtain an accurate and complete dynamic model in practice since many diverse sensors need to be utilized to obtain and identify system parameters. The model-free strategies are designed without considering the exoskeleton's dynamics model and their performance is influenced normally by the external disturbances [6]. The disturbances existing in the system have effects on the performance of the exoskeleton system.

To improve the robustness and accuracy of gait training, numerous strategies for wearable robotic exoskeletons have been substantially developed, such as robust control [7], and adaptive control [8]. However, those mentioned control approaches can only ensure asymptotic convergence when dealing with uncertainties and disturbances. To achieve consistent high dynamic tracking control and better convergence performance, the finite-time control strategy, such as sliding mode control (SMC), has been studied for the robotic exoskeleton control [9], [10]. SMC has two specific features of disturbance rejection and insensibility to uncertainties by designing the sliding mode surface [11]. Different types of

The associate editor coordinating the review of this manuscript and approving it for publication was Ning Sun .

SMC strategies are employed for robotic exoskeletons, such as terminal SMC [12], nonsingular terminal SMC [13] and fuzzy SMC [14]. Nevertheless, the performance of sliding mode control is susceptible to the existence of a chattering phenomenon, which may increase control effort and excite high-frequency oscillation [15]. The boundary layer saturation method is used to attenuate or eliminate the chattering. Meanwhile, this method will increase the error and reduce the speed of response.

In the real exoskeleton control, the internal such as chattering in the SMC or external disturbances exist universally and need to be compensated or suppressed for good performance. The unknown disturbances can be estimated by designing a disturbance observer and canceled in the feedback control law or be compensated by applying a disturbance compensator [16], [17]. To ensure a more transparent, effective and robust control strategy for robotic exoskeletons, one of the ordinary solutions is to use extended state observers (ESOs), which is designed to estimate the system states as well as total disturbances [9]. The ESO-based control approach is first to assess the disturbance in terms of the output and then canceled by its estimates [18]. The ESO is the core of active disturbance rejection control (ADRC). The central objective of active disturbance rejection control (ADRC) is to treat the internal and external uncertainties as a total disturbance and eliminate them actively [19]. ADRC has been employed successfully in the robotic exoskeleton control [20], [21]. The SMC combination with disturbance observer is efficient and useful for the disturbance rejection and the chattering phenomena elimination simultaneously [22]. Chen *et al.* employ the ADRC and terminal SMC into following the human gait trajectory in the lower extremity exoskeleton [21]. This method applied FTSMC to replace the ordinary control law of the ADRC and increase the fast response. However, this designed ADRC-based SMC strategy is only restricted to the swing phase and only the experiments of the swing leg are conducted.

To control the robotic system safely and robustly, the nonlinear terminal sliding mode control (N-TSMC) is employed to control the robotic system fast and robustly. Meantime, the ESO can estimate the internal or external disturbances, including the chattering or disturbance caused by the N-TSMC. The disturbances estimation can be eliminated or alleviated as the negative feedback in the control strategy design. The feedforward compensation control is added into the combination strategy to provide a fast response of the system. Given this, a novel ESO-based nonlinear terminal sliding mode control with feedforward compensation control (ESO-F-NTSMC) is employed to control the wearable exoskeleton with a robust response and fast convergence. Unlike the design principle in [21], the F-NTSMC is the primary and fundamental control law. The usage of ESO is helpful to estimate the total disturbance including that caused by chattering. The proposed control strategy is not restricted only to the swing leg and valid for the whole lower extremity in the stance swing and the swing phase.

In this paper, the lower extremity exoskeleton system is specified in the second section. In the third section, the proposed control strategy is presented. Experiments and results analysis are given in the fourth section. Conclusions are drawn in the final quarter.

## II. SYSTEM OVERVIEW

### A. THE LOWER EXTREMITY EXOSKELETON SPECIFICATION

Exoskeletons are worn by humans and work parallel with the human body as anthropomorphic devices [23]. Human motion analysis is usually used to design and optimize an assistive lower limb exoskeleton [24]. The designed exoskeleton needs to meet the natural movement's basic requirements, including enough range of motion, dexterous workspace, and lightweight [25]. A single leg is composed of three joints (hip, knee and ankle) and has seven degrees of freedom (DoF) for a human user, in which the hip joint has three DoFs, the knee joint has one DoF, and the ankle joint has three DoFs. To achieve and improve the comfortable wearing feeling, the designed lower extremity exoskeleton should have the same or close DoFs as the human legs have. The lower extremity mainly helps human people walk in the sagittal plane. To maintain the wearer's balance in the sagittal plane and take consideration of lightweight design, the flexion/extension DOFs of the hip joint and the knee joint are powered by DC motors.

The mechanical structure of the lower extremity is shown in Fig. 1. The powered hip joint or knee joint is actuated by a DC motor system encompassing an actuation motor and a gear pair with embedded encoders. The thigh segment, the shank segment and the waist part can be adjusted as required. The attachment straps on the thigh and the shank are made of soft materials to prevent the human leg's improper pressure from causing wearing discomfort. The wearable shoe is connected with the shank segment through the ankle joint and is similar to the real sports shoes to enhance flexibility. There are three pressure sensors to collect ground reaction force for phase identification. The designed exoskeleton can walk at the maximum speed of 1.25m/s and the weight of the whole system is less than 12kg. The exoskeleton can be worn by people whose weight is less than 80kg.

### B. MODELING FOR LOWER EXTREMITY EXOSKELETON

In the dynamic modeling, the lower extremity mainly moves in the sagittal plane. The powered DoFs are the flexion/extension movement of the hip joint and the knee joint. As the ankle joint's movement range is small in the sagittal plane, it can be regarded as a fixed joint in the model. Some parameters, such as the mass and length of the leg segment, are assumed to be constant. The leg segment of the exoskeleton can be simplified as a 2-DoFs link with the trunk as the fixed platform. Without loss of generality, the mathematical model of a single leg of the exoskeleton can be expressed as follows

$$M(q)\ddot{q} + C(q, \dot{q})\dot{q} + G(q) + D = T \quad (1)$$



**FIGURE 1.** The structure of the exoskeleton. HAA = hip adduction/abduction, HFE = hip flexion/extension, HML = hip medial/lateral rotation, KFE = knee flexion/extension, APD = ankle plantarflexion/dorsiflexion, APE = ankle pronation/external rotation; WLA = waist length adjustment, TLA = thigh length adjustment, SLA = shank length adjustment. The HFE and KFE DoFs are powered by DC motors and other DoFs are passive. The waist part can be adjusted up to 38cm. The length of the thigh and shank segments can be adjusted to fit the human user in the height of 155cm-185cm.

where  $M(q) \in R^{2 \times 2}$  is the symmetric definite inertial matrix;  $C(q, \dot{q}) \in R^{2 \times 2}$  is the Coriolis and Centrifugal force matrix;  $G(q) \in R^{2 \times 1}$  is the gravitational force matrix;  $T \in R^{2 \times 1}$  is the control input torque vector;  $D = [D_1, D_2]^T$  denotes un-modeled dynamics and external disturbances;  $q = [q_h \ q_k]^T$ ,  $\dot{q} = [\dot{q}_h \ \dot{q}_k]^T$ ,  $\ddot{q} = [\ddot{q}_h \ \ddot{q}_k]^T$ , where  $q_h$  and  $q_k$  are angles for the hip joint and the knee joint respectively;  $T = [T_h \ T_k]^T$  is input torque vector,  $T_h$  is driving torque of the hip joint while  $T_k$  is driving torque of the knee joint. The specific expression of matrices of  $M(q)$ ,  $C(q, \dot{q})$  and  $G(q)$  can be shown as the following [26]

$$\begin{cases} M(q) = \begin{bmatrix} M_{11}(q) & M_{12}(q) \\ M_{21}(q) & M_{22}(q) \end{bmatrix} \\ C(q, \dot{q}) = \begin{bmatrix} C_{11}(q, \dot{q}) & C_{12}(q, \dot{q}) \\ C_{21}(q, \dot{q}) & C_{22}(q, \dot{q}) \end{bmatrix} \\ G(q) = \begin{bmatrix} G_1(q) \\ G_2(q) \end{bmatrix} \end{cases} \quad (2)$$

### III. THE ESO-F-NTSMC STRATEGY DESIGN

#### A. HUMAN GAIT GENERATION METHOD

The lower extremity exoskeleton is a human in the loop system, which needs to adjust the robot system and the human user in coordination. The exoskeleton system needs to understand how the human user moves. The exoskeleton's control process has two significant aspects: one is to generate human gait trajectory based on sensors measurement information. The other is to shadow the human gait by designing a control strategy taking care of the user's properties. Human gait trajectory generation is the essence and the first step of exoskeleton control. In this paper, the human gait is obtained by the combination of the pressure sensors and IMUs. The proposed

human gait generation method is based on walking phase identification. In this work, the walking phases are separated into the stance phase and the swing phase. Those two walking phases can be distinguished by a concise threshold method [27].

*Definition 1:* The ground reaction force (GRF) measured by pressure sensors can be recorded as  $F_{L,1}(0)$ ,  $F_{L,2}(0)$ ,  $F_{L,3}(0)$ ,  $F_{R,1}(0)$ ,  $F_{R,2}(0)$ , and  $F_{R,3}(0)$  for the left leg and right leg respectively in the initial stance phase.

*Definition 2:* The sums of GRF in those two shoes are expressed as follows

$$\begin{aligned} F_{la}(0) &= F_{l1}(0) + F_{l2}(0) + F_{l3}(0) \\ F_{ra}(0) &= F_{r1}(0) + F_{r2}(0) + F_{r3}(0) \end{aligned} \quad (3)$$

where  $F_{la}(0)$  and  $F_{ra}(0)$  are the initial sums of GRFs when the human user stands upright. In real-time, the GRF sums in the  $k$ th interval are shown as below

$$\begin{aligned} F_{la}(k) &= F_{l1}(k) + F_{l2}(k) + F_{l3}(k) \\ F_{ra}(k) &= F_{r1}(k) + F_{r2}(k) + F_{r3}(k) \end{aligned} \quad (4)$$

*Definition 3:* Several positive weight parameters are defined as  $\alpha_l$ ,  $\beta_l$ ,  $\alpha_r$  and  $\beta_r$  to satisfy  $\alpha_l < 1 < \beta_l$  and  $\alpha_r < 1 < \beta_r$ .

*Lemma 1* [27]: The phase identification process is divided into three cases, which is shown as the following,

*Case 1: double stance for two legs*

$$\begin{aligned} \alpha_l F_{la}(0) &\leq F_{la}(k) \leq \beta_l F_{la}(0) \text{ or } F_{la}(k) > \beta_l F_{la}(0) \\ \alpha_r F_{ra}(0) &\leq F_{ra}(k) \leq \beta_r F_{ra}(0) \text{ or } F_{ra}(k) > \beta_r F_{ra}(0) \end{aligned} \quad (5)$$

*Case 2: stance phase for left and swing phase for right*

$$\begin{aligned} F_{la}(k) &> \beta_l F_{la}(0) \text{ or } \alpha_l F_{la}(0) \leq F_{la}(k) \leq \beta_l F_{la}(0) \\ F_{ra}(k) &< \alpha_r F_{ra}(0) \end{aligned} \quad (6)$$

Case 3: swing phase for left and stance phase for right

$$\begin{aligned}
 F_{la}(k) &< \alpha_l F_{la}(0) \\
 F_{ra}(k) &> \beta_r F_{ra}(0) \text{ or } \alpha_r F_{ra}(0) \leq F_{ra}(k) \leq \beta_r F_{ra}(0) \quad (7)
 \end{aligned}$$

Remark 1: As discussed above in Lemma 1, the walking phases for a single leg can be identified as the stance phase and the swing phase. The proposed gait generation method is built on the foundation of phase identification.

Definition 4: Except for double stance, the gait trajectory in other phases can be acquired by the IMU measurement directly as following

$$\begin{aligned}
 \theta_h(k+1) &= \theta_h(k) + \Delta\theta_h(k) \\
 \theta_k(k+1) &= \theta_k(k) + \Delta\theta_k(k) \quad (8)
 \end{aligned}$$

Remark 2:  $\theta_h(k+1)$  and  $\theta_h(k)$  are the hip joint angle in the  $(k+1)$  interval and the  $k$  interval respectively, while  $\theta_k(k+1)$  and  $\theta_k(k)$  are the knee joint angle in the  $(k+1)$  interval and the  $k$  interval respectively.  $\Delta\theta_h(k)$  and  $\Delta\theta_k(k)$  are the increment angular position obtained from the IMU attached on the thigh and the shank respectively.

Remark 3: The IMU's original output has been processed by the extended Kalman filter to improve accuracy [28]. According to the placement of IMUs,  $\Delta\theta_h(k)$  or  $\Delta\theta_k(k)$  in Eq. (11) is the yaw angle relative to the upright posture.

$$\begin{aligned}
 \Delta\theta_h(k) &= \begin{cases} \Delta\theta_{lh}(k) & \text{in swing phase} \\ 0 & \text{in stance phase} \end{cases} \\
 \Delta\theta_k(k) &= \begin{cases} \Delta\theta_{lk}(k) & \text{in swing phase} \\ 0 & \text{in stance phase} \end{cases} \quad (9)
 \end{aligned}$$

where  $\Delta\theta_{lh}(k)$  and  $\Delta\theta_{lk}(k)$  can be measured by the IMUs attached to the thigh and the shank respectively. If the phase is identified as the stance phase,  $\Delta\theta_{lh}(k)$  and  $\Delta\theta_{lk}(k)$  will be set as zero.

### B. ESO FOR LOWER EXTREMITY EXOSKELETON

Based on the previous work in [26], the process of ESO derivation is expressed in detail. In general, a second order, single input and single output (SISO) with known knowledge can be expressed as the following:

$$\ddot{y} = -a_1\dot{y} - a_0y + f_0 + bu \quad (10)$$

where  $\ddot{y}$ ,  $\dot{y}$  and  $y$  are the acceleration, velocity and position of the system,  $a_1$  and  $a_0$  are the known knowledge of the system,  $f_0$  is the external disturbance and the un-modeled dynamics,  $u$  is the input of the controller,  $b$  is a parameter dependent on the system. The system state can be defined as  $x_1 = y$ ,  $x_2 = \dot{y}$  and  $x_3 = -a_1\dot{y} - a_0y + f_0$ . The system can be rewritten as the following expression

$$\begin{cases} \dot{x}_1 = x_2 \\ \dot{x}_2 = x_3 + bu \\ \dot{x}_3 = -a_1x_3 - a_0x_2 - a_1bu + h \end{cases} \quad (11)$$

Defining the observation states as  $z_1 = x_1$ ,  $z_2 = x_2$  and  $z_3 = x_3$ , then the formulation (11) can be rewritten as follows:

$$\begin{cases} \dot{z}_1 = z_2 \\ \dot{z}_2 = z_3 + bu \\ \dot{z}_3 = -a_1z_3 - a_0z_2 - a_1bu \end{cases} \quad (12)$$

The observation error is defined as  $e_o = \tilde{z}_1 - z_1$ , where  $\tilde{z}_1$  is the state estimation. The ESO can be expressed as below:

$$\begin{cases} \dot{\tilde{z}}_1 = \tilde{z}_2 + l_1e_o \\ \dot{\tilde{z}}_2 = \tilde{z}_3 + bu + l_2e_o \\ \dot{\tilde{z}}_3 = -a_1\tilde{z}_3 - a_0\tilde{z}_2 - a_1bu + l_3e_o \end{cases} \quad (13)$$

where  $l_1$ ,  $l_1$  and  $l_1$  are constant are positive constant parameters relative to the bandwidth of the controller and observer. Through the usage of ESO in Eq. (13), the total disturbances can be estimated and then eliminated in the feedback law design. Similarly, the mathematical model of the exoskeleton is a second-order multi-input and multi-output (MIMO) system.

Definition 5: Based on Eq. (1) - Eq. (5), the dynamics model of the exoskeleton can be rewritten as below

$$\begin{cases} M_{11}\ddot{q}_h + M_{12}\ddot{q}_k + C_{11}\dot{q}_h + C_{12}\dot{q}_k + G_1 + D_1 = T_h \\ M_{21}\ddot{q}_h + M_{22}\ddot{q}_k + C_{21}\dot{q}_h + C_{22}\dot{q}_k + G_2 + D_2 = T_k \end{cases} \quad (14)$$

Based on Eq. (14), the following expression in state space can be obtained.

$$\begin{cases} \ddot{q}_h = 1/(M_{11}M_{22} - M_{21}M_{12})^*(M_{22}T_{11} - M_{12}T_{21} - F_1) \\ \ddot{q}_k = 1/(M_{12}M_{21} - M_{11}M_{22})^*(M_{21}T_{11} - M_{11}T_{21} - F_2) \end{cases} \quad (15)$$

Remark 4:

$$\begin{cases} F_1 = (M_{22}C_{11} - M_{12}C_{21})\dot{q}_h + (M_{22}C_{12} - M_{12}C_{22})\dot{q}_k \\ \quad + M_{22}G_1 - M_{12}G_2 + M_{22}D_1 - M_{12}D_2 \\ F_2 = (M_{21}C_{11} - M_{11}C_{21})\dot{q}_h - (M_{21}C_{12} - M_{11}C_{22})\dot{q}_k \\ \quad - M_{21}G_1 + M_{11}G_2 - M_{21}D_1 + M_{11}D_2 \end{cases} \quad (16)$$

Eq. (16) can be expressed as

$$\begin{aligned}
 \ddot{q}_h &= C_{f1}^*(M_{22}T_1 - M_{12}T_2) + f_1 \\
 \ddot{q}_k &= -C_{f1}^*(M_{21}T_1 - M_{11}T_2) + f_2 \quad (17)
 \end{aligned}$$

where  $C_{f1} = 1/(M_{11}M_{22} - M_{21}M_{12})$ ,  $f_1 = -F_1C_{f1}$ ,  $f_2 = C_{f1}F_2$ .

Definition 6: Then define a positive matrix as

$$D = \begin{bmatrix} C_{f1}M_{22} & 0 \\ 0 & C_{f1}M_{11} \end{bmatrix} \quad (18)$$

The system Eq. (17) can be rewritten as

$$\ddot{\mathbf{q}} = \mathbf{f} + \mathbf{U} \quad (19)$$

where  $\ddot{\mathbf{q}} = [\ddot{q}_h, \ddot{q}_k]^T$ ,  $\mathbf{f} = [f_1, f_2]^T$ ,  $\mathbf{U} = [U_1, U_2]^T = D[T_1, T_2]^T$ .

Given that  $\mathbf{U}$  is known, the control input  $\mathbf{T} = [T_1, T_2]^T$  can be obtained as  $\mathbf{T} = \mathbf{D}^{-1}\mathbf{U} = \mathbf{D}_{inv}\mathbf{U}$ . Then Eq. (19) can be split into two equations as the following

$$\ddot{q}_h = f_1 + \mathbf{D}_{inv}(1, 1) \cdot U_1 \ddot{q}_k = f_2 + \mathbf{D}_{inv}(2, 2) \cdot U_2 \quad (20)$$

Based on the general formula of ESO and Eq. (20), two ESOs can be obtained for the hip joint and the knee joint respectively as follows

$$\begin{cases} \dot{z}_1 = z_2 + l_1 e_1 \\ \dot{z}_2 = \mathbf{D}_{inv}(1, 1)U_1 + z_3 + l_2 e_1 \\ \dot{z}_3 = l_3 e_1 \\ \dot{z}_4 = z_5 + l_4 e_2 \\ \dot{z}_5 = \mathbf{D}_{inv}(2, 2)U_2 + z_6 + l_5 e_2 \\ \dot{z}_6 = l_6 e_2 \end{cases} \quad (21)$$

*Remark 5:*  $L_1 = [l_1, l_2, l_3]^T$  and  $L_2 = [l_4, l_5, l_6]^T$  are the positive observer gain matrices,  $[\tilde{z}_3, \tilde{z}_6]^T$  can be obtained from  $[z_3, z_6]^T$  as the estimated disturbances by ESO. The designed ESO can estimate total disturbance by the extended state calculation.

### C. ESO-F-NTSMC STRATEGY DESIGN

In general, the SMC for systems can be achieved by the sliding surface definition and the control law design. The proposed control approach aims at improving the whole performance with high accuracy and fast coverage. The tracking error in the nonlinear SMC strategy can converge to zero in finite time [29], [30]. As discussed previously, the designed target trajectory is the human gait as  $q_d = [\theta_h \ \theta_k]^T$  in Eq. (11) and the actual position feedback is  $q = [q_h \ q_k]^T$ . The tracking errors of the hip joint and the knee joint can be defined as below

$$e = q_d - q = [\theta_h - q_h, \theta_k - q_k]^T \quad (22)$$

*Definition 7:* To ensure that the tracking errors converge within finite-time and avoid the singular problem, the sliding mode surface can be designed as [31]

$$s = \dot{e} + a_1 \text{sign}(e) |e|^{\lambda_1} + a_2 \text{sign}(e) |e|^{\lambda_2} \quad (23)$$

*Remark 6:*  $a_1$  and  $a_2$  are positive parameters,  $\lambda_1 \geq 1, 0 < \lambda_2 < 1$ . Based on Eq. (22), in order to improve robustness and fast convergence of the SMC, a designed nonlinear fast terminal sliding surface is represented as follows

$$s = \dot{e} + a_1 \text{sign}(e) |e|^{\lambda_1} + a_2 \text{sign}(e) |e|^{\lambda_2} + h \int_0^{ts} edt \quad (24)$$

where  $h$  is a positive definite matrix,  $ts$  is the sampling cycle time. The time derivative of the sliding surface is expressed as the following

$$\dot{s} = \ddot{e} + a_1 r_1 |e|^{\lambda_1-1} \dot{e} + a_2 r_2 |e|^{\lambda_2-1} \dot{e} + he \quad (25)$$

The control laws should be chosen to satisfy the existence condition of SMC  $s^T \dot{s} < 0$  and the exponent reaching law is given as follows

$$\dot{s} = -\epsilon \text{sgn}(s) - \mathbf{K}s \quad (26)$$

where  $\epsilon$  and  $\mathbf{K}$  are positive definite matrices,  $\text{sgn}(s)$  is a symbolic function which is shown as the following

$$\text{sgn}(s) = \begin{cases} 1, & s > 0 \\ 0, & s = 0 \\ -1, & s < 0 \end{cases} \quad (27)$$

*Theorem 1:* Combining Eq. (24) and Eq. (26),

$$\ddot{e} + a_1 \lambda_1 |e|^{\lambda_1-1} \dot{e} + a_2 \lambda_2 |e|^{\lambda_2-1} \dot{e} + he = -\epsilon \text{sgn}(s) - \mathbf{K}s \quad (28)$$

Based on Eq. (21),  $\ddot{e} = \ddot{q}_d - \ddot{q}$  and Eq. (19),  $\ddot{q} = \mathbf{f} + \mathbf{U}$ , then Eq. (28) can be rewritten as

$$\ddot{q}_d - \mathbf{f} - \mathbf{U} + a_1 \lambda_1 |e|^{\lambda_1-1} \dot{e} + a_2 \lambda_2 |e|^{\lambda_2-1} \dot{e} + he = -\epsilon \text{sgn}(s) - \mathbf{K}s \quad (29)$$

Based on Eq. (29), the control vector can be obtained as below

$$\mathbf{U} = \ddot{q}_d - \mathbf{f} + a_1 \lambda_1 |e|^{\lambda_1-1} \dot{e} + a_2 \lambda_2 |e|^{\lambda_2-1} \dot{e} + he + \epsilon \text{sgn}(s) + \mathbf{K}s \quad (30)$$

The proposed controller should guarantee that the tracking error and the sliding surface can converge to zero asymptotically. If  $t \rightarrow \infty, e \rightarrow 0, s \rightarrow 0$ , then the control system is globally stable, i.e., when  $t \rightarrow \infty, e \rightarrow 0, s \rightarrow 0$ . The Lyapunov-based stability proof is presented as the following.

*Proof 1:* The Lyapunov function can be defined as

$$\mathbf{V} = \frac{1}{2} \mathbf{s}^T \mathbf{s} \quad (31)$$

The differentiation of  $\mathbf{V}$  can be denoted as follows

$$\dot{\mathbf{V}} = \mathbf{s}^T \dot{\mathbf{s}} \quad (32)$$

Combining Eq. (23) and Eq. (26)

$$\begin{aligned} \dot{\mathbf{V}} &= \mathbf{s}^T \dot{\mathbf{s}} = \mathbf{s}^T \left( \ddot{q}_d - \ddot{q} + a_1 \lambda_1 |e|^{\lambda_1-1} \dot{e} + a_2 \lambda_2 |e|^{\lambda_2-1} \dot{e} + he \right) \\ &= \mathbf{s}^T \left( \ddot{q}_d - (\mathbf{f} + \mathbf{U}) + a_1 \lambda_1 |e|^{\lambda_1-1} \dot{e} + a_2 \lambda_2 |e|^{\lambda_2-1} \dot{e} + he \right) \end{aligned} \quad (33)$$

Substituting Eq. (30) into Eq. (33), we can obtain

$$\dot{\mathbf{V}} = \mathbf{s}^T (-\epsilon \text{sgn}(s) - \mathbf{K}s) = -\mathbf{s}^T \epsilon \text{sgn}(s) - \mathbf{s}^T \mathbf{K}s \quad (34)$$

As discussed above,  $\sigma, \mathbf{K}$  and  $\epsilon$  are positive, then  $\mathbf{s}^T \epsilon \text{sgn}(s)$  and  $\mathbf{s}^T \mathbf{K}s$  are also positive, finally  $\dot{\mathbf{V}} < 0$ .

*Remark 7:* Therefore, the control system is globally stable, which means when  $s \rightarrow 0$  as  $t \rightarrow \infty$ , then  $e \rightarrow 0$  and  $\dot{e} \rightarrow 0$  as  $t \rightarrow \infty$ . According to the stability proof, the trajectory tracking error can converge to zero by the proposed control law. Based on Eq. (30), the control input to the lower extremity is shown as below

$$\begin{aligned} \mathbf{T} &= \mathbf{D}^{-1}\mathbf{U} \\ &= \mathbf{D}^{-1} \left( \ddot{q}_d - \mathbf{f} + a_1 \lambda_1 |e|^{\lambda_1-1} \dot{e} + a_2 \lambda_2 |e|^{\lambda_2-1} \dot{e} + he + \epsilon \text{sgn}(s) + \mathbf{K}s \right) \end{aligned} \quad (35)$$

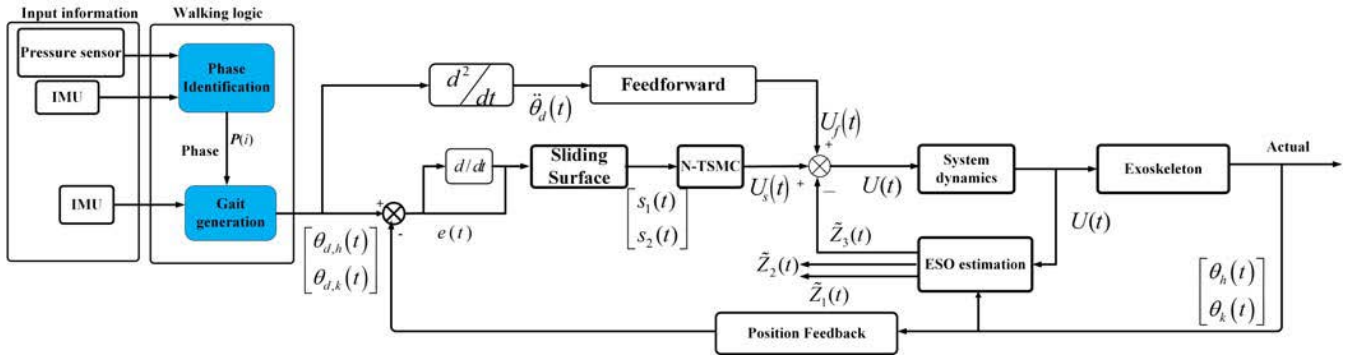


**FIGURE 2.** The proposed ESO-F-NTSMC strategy for the lower extremity exoskeleton. The input part mainly includes information from pressure sensors and IMU. The walking logic part describes the walking phase identification and the human gait generation. The ESO estimates the disturbances as negative feedback into the master control signals. The main function of the designed control strategy is to shadow the human gait trajectory.

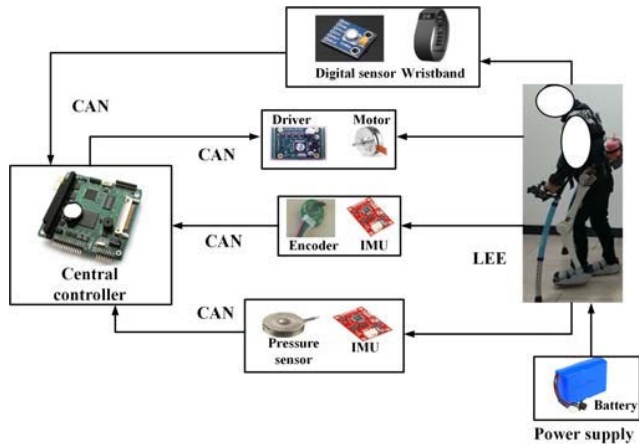


**FIGURE 3.** Hardware architecture of the exoskeleton control system. All distributed slaves communicate with the central PC through CAN bus. Those sensors are plugged into the CAN network to transfer information.

where  $\mathbf{D}$  is expressed in Eq. (18). In the robot control, the feedforward control can provide a fast response.

*Remark 8:* When the walking phase and the motion direction of the leg segment change, discontinuous friction or inertial will encounter affecting the human gait tracking performance. To cope with these erratic changes and assure a smooth transient response, a feedforward control loop is added into the nonlinear SMC expressed in Eq. (35)

$$\begin{aligned} \mathbf{T} = & \mathbf{M}\ddot{\mathbf{q}}_d + \mathbf{C}(\mathbf{q}_d, \dot{\mathbf{q}}_d)\dot{\mathbf{q}}_d \\ & + \mathbf{D}^{-1} \left( \ddot{\mathbf{q}}_d - \mathbf{f} + a_1\lambda_1 |e|^{\lambda_1-1} \dot{e} + a_2\lambda_2 |e|^{\lambda_2-1} \dot{e} \right. \\ & \left. + he + \varepsilon \text{sgn}(s) + \mathbf{K}s \right) \end{aligned} \quad (36)$$

The framework of the proposed ESO-F-NTSMC strategy is shown in Fig. 2.

## IV. EXPERIMENTS

### A. CONTROL ARCHITECTURE

The control architecture of the lower extremity exoskeleton system is shown in Fig. 3. As Fig. 3 shows, the central controller is an embedded PC, whose function is to produce control signals, receive the sensor feedback information and transfer relevant information to other modules. A single leg

has two actuation systems, each of which is composed of a driver and a DC motor. There are two kinds of sensors employed in the control framework, i.e., inertial measurement unit (IMU) and position sensor encoder. The IMU is embedded in the attachment point and the encoder is integrated into the DC motor. There are three pressure sensors in the wearable shoe and one IMU sensor attached to the shoe’s side. The improvement of measurement accuracy can be achieved by the compensation of the information fusion algorithm. In this kind of used IMU, the extended Kalman filter is used to deal with the problem of time drift and accurate output data in real-time. All sensors are transferred back into the central controller through the CAN bus. The control command signals are also transmitted through the CAN bus. The power supply is provided by the 24V lithium battery. Besides, some digital sensors are used to start on/off the system or as safety switches. A wearable watch is also utilized as a measurement tool to obtain the kinematic information of the lower extremity exoskeleton. Some safety precautions are taken into consideration in mechanical design and electrical design. In the mechanical design, physical status indicator switches are placed to prevent leg segments from excessive excursions. In the electrical system, a sizeable e-stop button shuts off full power and the motor control torque is limited by using a saturation function.

### B. EXPERIMENTAL SETUP

Experiments are performed to evaluate the performance of the proposed approach. Three human volunteers participated in the experiments and the Laboratory Management Council authorized ethical approval. Those three human volunteers have an average height of  $1.70 \pm 0.5$  m, an average weight of  $65 \pm 4.5$  kg and an average age of  $33 \pm 5$  years old. The lower extremity functions of all human subjects are normal. The lower extremity exoskeleton is used with crutches’ help to imitate the usage scenario of patients, which is shown in Fig. 4. The human volunteers are asked to wear the exoskeleton by himself as the following process: (1) wear the exoskeleton and adjust the leg segment to fit the human user’s body shape; (2) fasten all belts to make the user feel comfortable, especially the attachment points on the leg;

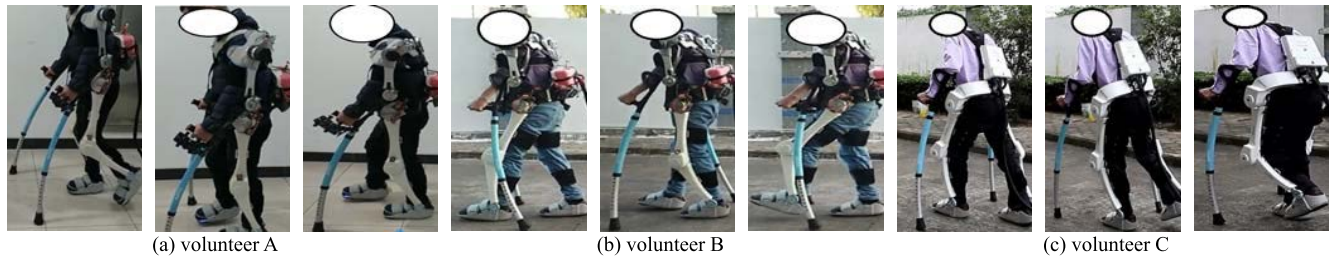


FIGURE 4. Experiments of wearing the lower extremity exoskeleton for straight walking on the floor. The crutches were used for walking safety.

(3) adjust the exoskeleton until to prepare to walk; (4) prepare the assistive crutches; (5) press down the turn on/off button to start on the actuation system; (6) walk on the ground at a natural mode. During the experiments, the kinematic and kinetic data are collected in real-time through the user software interface.

We compare three kinds of control strategies: traditional terminal SMC (TSMC), ESO-based traditional terminal SMC (ESO-TSMC) and the proposed approach (ESO-F-NTSMC). In the TSMC, the sliding surface is defined as Eq. (23) shows and the control law can be expressed as follows

$$\mathbf{T} = \mathbf{M}(\mathbf{q}) \left( \ddot{\mathbf{q}}_d + a_1 r_1 |e|^{r_1-1} \dot{e} + a_2 r_2 |e|^{r_2-1} \dot{e} + \varepsilon \operatorname{sgn}(s) + \mathbf{K}s \right) + \mathbf{c}(\mathbf{q}, \dot{\mathbf{q}})\dot{\mathbf{q}} + \mathbf{G}(\mathbf{q}) + \mathbf{f} \quad (37)$$

The formula of ESO-TSMC can be shown as below

$$\mathbf{T} = \mathbf{D}^{-1} \left( \ddot{\mathbf{q}}_d - \mathbf{f} + a_1 r_1 |e|^{r_1-1} \dot{e} + a_2 r_2 |e|^{r_2-1} \dot{e} + \varepsilon \operatorname{sgn}(s) + \mathbf{K}s \right) \quad (38)$$

In this experiment, three kinds of strategies, namely, TSMC, ESO-TSMC and the proposed ESO-F-NTSMC, are compared from the perspective of the target trajectory tracking performance. To ensure the performance comparison's validation, all the parameters are predefined as the same, including parameters of ESO and TSMC. Those parameters in ESO can be obtained from the observer's bandwidth and all matrices in TSMC are symmetric. To make the difference more explicit, the root mean square error (RSME) is utilized to evaluate the strategy's performance as follows

$$RSME = \sqrt{\sum_{k=1}^N \|e(k)\|^2 / N} \quad (39)$$

where  $e(k)$  is the  $k$ th sampling tracking error and  $N$  is the size of the error vector.

### C. EVALUATION AND RESULTS ANALYSIS

The wearers are asked to walk at a natural speed. Based on the online gait generation method by Eq. (6) - Eq. (12), the target human gait trajectory can be obtained. The position encoder monitors the actual angular position of the hip joint and the knee joint. Three subjects carried out the wearing experiments and the target trajectory may be different because of individual differences. The target trajectory can be generated based on the proposed online gait generation method, as shown in Fig. 5. Fig. 5 shows the mean joint

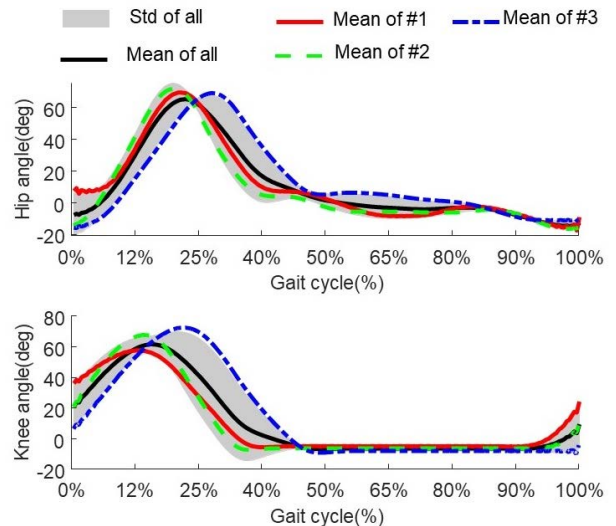


FIGURE 5. The target trajectory for the three subjects under the proposed human gait generation method.

trajectories of the hip joint and knee joint for the three subjects and gives the mean value and standard deviation for all three subjects. In a whole gait cycle, the gait trajectory can automatically be transferred from the stance phase to the swing phase. The human gait trajectory tracking performance by using the proposed method, ESO-F-NTSMC, is illustrated in Fig. 6. The human gait generation method obtains the target gait trajectory and the embedded encoder receives the actual trajectory feedback. As Fig. 6 depicts, the gait tracking is quite good and the target gait trajectory can be followed. It is evident that the proposed strategy can shadow the human gait trajectory in time and accurately for the lower extremity exoskeleton. Fig. 6 also illustrates the consistency of the proposed method for different users.

To illustrate the validity of the proposed method well, the RSME and tracking errors are compared among TSMC, ESO-TSMC and ESO-F-NTSMC. The comparisons of tracking performance are conducted, as shown in Fig. 7 and Fig. 8. As Fig. 7 shows, the RSME is regarded as the comparison index for those three strategies. RSMEs of two joints in TSMC are larger than 0.4 degrees while those in ESO-TSMC and ESO-F-NTSMC are smaller than 0.3 degrees. The RSMEs in ESO-F-NTSMC are smaller than those in ESO-TSMC obviously. From the perspective of the tracking error, depicted in Fig. 8, the ESO-F-NTSMC can

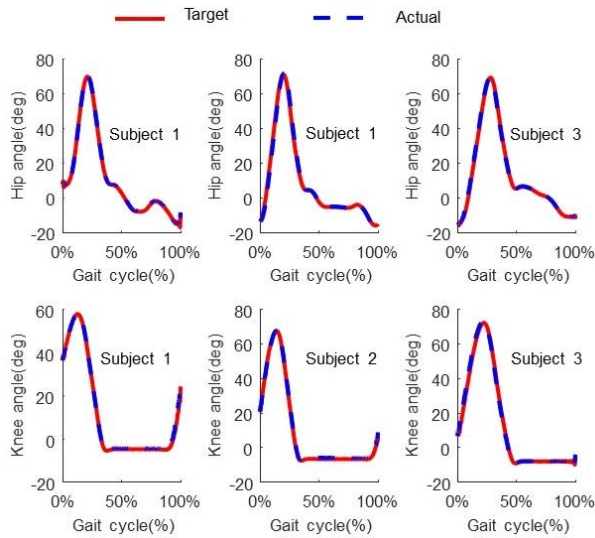


FIGURE 6. Trajectory tracking performance by the proposed method.

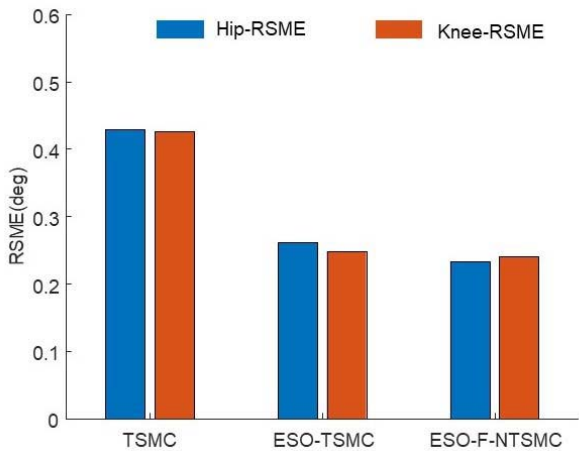


FIGURE 7. The RSME performance comparison for three strategies.

obtain the most accurate tracking compared with the other two strategies. In Fig. 7 and Fig. 8, the tracking errors are the mean values for three subjects. A more detailed comparison is conducted in Table 1. Table 1 gives the tracking errors' range of hip joint and knee joint and provides performance improvement from the perspective of RSMEs. Compared with the traditional TSMC, the ESO-TSMC and ESO-F-NTSMC have 41.49% and 47.04% performance improvement for the hip joint and 42.04% and 44.02% for the knee joint respectively. To some extent, the proposed method is effective for different wearers and the exoskeleton system can be adopted to help different users. The usage of ESO can provide more accurate and robust trajectory tracking for the LEE. The ESO-F-NTSMC has a small improvement than ESO-TSMC.

In addition, the control torque comparison is also depicted, as shown in Fig. 9. The control torque is estimated by the control current feedback and the relationship between the control torque and the control current is assumed to be approximately linear. As Fig. 9 shows, the chattering phenomenon

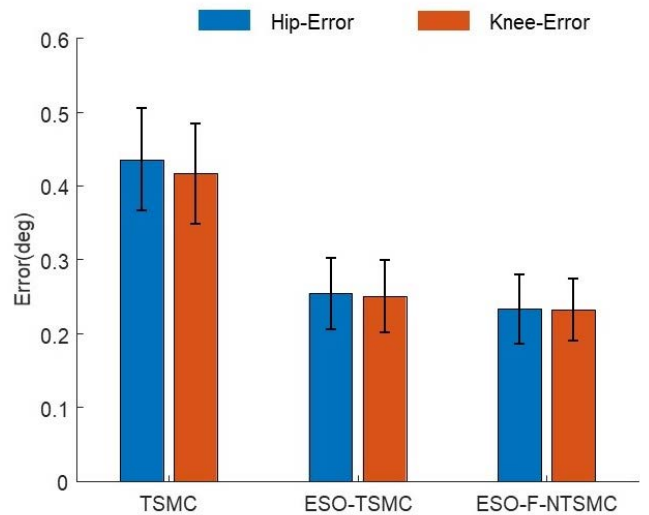


FIGURE 8. The tracking error comparison for three strategies.

TABLE 1. The comparison among three control strategies.

Strategy	Tracking error (degree)		Performance improvement	
	Hip joint	Knee joint	Hip joint	Knee joint
TSMC	(0.1907,0.6115)	(0.1693,0.5926)	-	-
ESO-TSMC	(0.1307,0.3575)	(0.1188,0.3753)	41.49%	42.04%
ESO-F-NTSMC	(0.1051,0.3234)	(0.1319,0.3346)	47.07%	44.02%

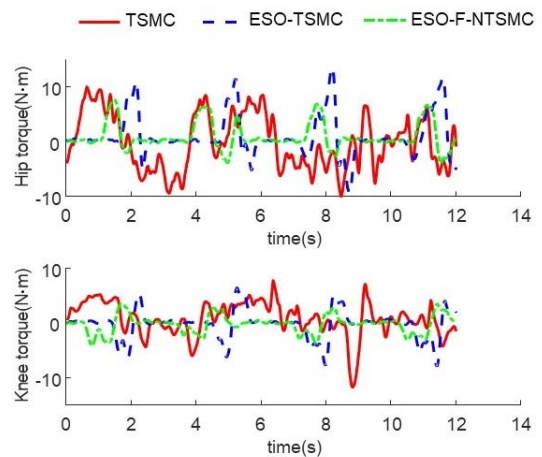


FIGURE 9. The control torque comparison for three strategies.

of ESO-TSMC or ESO-F-NTSMC is weaker than that of TSMC. The control torque of the ESO-F-NTSMC is smaller than that of TSMC and ESO-TSMC. The ESO-F-NTSMC has smoother movement and a more powerful ability to deal with the disturbances. Therefore, the proposed method can improve the gait tracking accuracy and overcome the total disturbances to promote the smoothness of movement.

#### D. DISCUSSION

The proposed method ESO-F-NTSMCT is used to track the human gait in real-time. Compared with TSMC, the proposed method is more robust and smoother. The proposed control



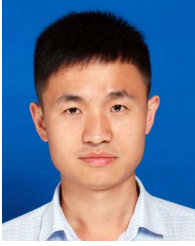
method has the potential to be a practical general control framework for the lower extremity exoskeleton because of its adaptation to different users and good application performance. Meantime, there is one significant issue for the proposed method in real usage, which is too many parameters need to be set and adjusted by empirical.

## V. CONCLUSION

In this work, we contributed to the development of a control approach for lower extremity exoskeleton, namely ESO-based nonlinear terminal SMC with feedforward compensation. The lower extremity exoskeleton under study and its mathematical model is given in detail. The control strategy design process is also presented, encompassing the human gait generation, the ESO derivation, the SMC design and the stability proof. Finally, the experiments are conducted on three human volunteers. The results show that the proposed method called ESO-F-NTSMC can obtain more precise tracking performance and smoother movement. The ESO-F-NTSMC strategy has the potential to achieve promising performance and can be implemented and extended to other rehabilitation exoskeletons control. Looking towards the future, we will study how to tune those parameters online to improve adaptability. The dynamic model will be identified by an online calculation method such as a neural network. The metabolic cost of wearing the exoskeleton will also be envisioned in future work.

## REFERENCES

- [1] A. B. Zoss, H. Kazerooni, and A. Chu, "Biomechanical design of the berkeley lower extremity exoskeleton (BLEEX)," *IEEE/ASME Trans. Mechatronics*, vol. 11, no. 2, pp. 128–138, Apr. 2006.
- [2] K. Gui, U.-X. Tan, H. Liu, and D. Zhang, "Electromyography-driven progressive assist-as-needed control for lower limb exoskeleton," *IEEE Trans. Med. Robot. Bionics*, vol. 2, no. 1, pp. 50–58, Feb. 2020.
- [3] S. M. Campbell, C. P. Diduch, and J. W. Sensinger, "Autonomous assistance-as-needed control of a lower limb exoskeleton with guaranteed stability," *IEEE Access*, vol. 8, pp. 51168–51178, 2020.
- [4] Y. Li, X. Guan, X. Han, Z. Tang, K. Meng, Z. Shi, B. Penzlin, Y. Yang, J. Ren, Z. Yang, Z. Li, S. Leonhardt, and L. Ji, "Design and preliminary validation of a lower limb exoskeleton with compact and modular actuation," *IEEE Access*, vol. 8, pp. 66338–66352, 2020.
- [5] W. Meng, Q. Liu, Z. Zhou, Q. Ai, B. Sheng, and S. S. Xie, "Recent development of mechanisms and control strategies for robot-assisted lower limb rehabilitation," *Mechatronics*, vol. 31, pp. 132–145, Oct. 2015.
- [6] Y. Su, D. Sun, L. Ren, and J. K. Mills, "Integration of saturated PI synchronous control and PD feedback for control of parallel manipulators," *IEEE Trans. Robot.*, vol. 22, no. 1, pp. 202–207, Feb. 2006.
- [7] C. Jarrett and A. J. McDaid, "Robust control of a cable-driven soft exoskeleton joint for intrinsic human-robot interaction," *IEEE Trans. Neural Syst. Rehabil. Eng.*, vol. 25, no. 7, pp. 976–986, Jul. 2017.
- [8] R. Lu, Z. Li, C.-Y. Su, and A. Xue, "Development and learning control of a human limb with a rehabilitation exoskeleton," *IEEE Trans. Ind. Electron.*, vol. 61, no. 7, pp. 3776–3785, Jul. 2014.
- [9] S. Zhu, X. Jin, B. Yao, Q. Chen, X. Pei, and Z. Pan, "Non-linear sliding mode control of the lower extremity exoskeleton based on human-robot cooperation," *Int. J. Adv. Robot. Syst.*, vol. 13, no. 5, pp. 1–10, Oct. 2016.
- [10] X. Wang, X. Li, J. Wang, X. Fang, and X. Zhu, "Data-driven model-free adaptive sliding mode control for the multi degree-of-freedom robotic exoskeleton," *Inf. Sci.*, vol. 327, pp. 246–257, Jan. 2016.
- [11] X.-G. Yan, S. K. Spurgeon, and C. Edwards, "Dynamic sliding mode control for a class of systems with mismatched uncertainty," *Eur. J. Control*, vol. 11, no. 1, pp. 1–10, Jan. 2005.
- [12] S. Han, H. Wang, and Y. Tian, "Model-free based adaptive nonsingular fast terminal sliding mode control with time-delay estimation for a 12 DOF multi-functional lower limb exoskeleton," *Adv. Eng. Softw.*, vol. 119, pp. 38–47, May 2018.
- [13] T. Madani, B. Daachi, and K. Djouani, "Non-singular terminal sliding mode control: Application to an actuated exoskeleton," *Mechatronics*, vol. 33, pp. 136–145, Feb. 2016.
- [14] X. L. Jin, S. Q. Zhu, X. C. Zhu, Q. C. Chen, and X. Q. Zhang, "Single-input adaptive fuzzy sliding mode control of the lower extremity exoskeleton based on human-robot interaction," *Adv. Mech. Eng.*, vol. 9, no. 2, pp. 1–9, Feb. 2017.
- [15] X. Hai, Z. Wang, Q. Feng, Y. Ren, B. Xu, J. Cui, and H. Duan, "Mobile robot ADRC with an automatic parameter tuning mechanism via modified pigeon-inspired optimization," *IEEE/ASME Trans. Mechatronics*, vol. 24, no. 6, pp. 2616–2626, Dec. 2019.
- [16] H. Pan, W. Sun, H. Gao, and X. Jing, "Disturbance observer-based adaptive tracking control with actuator saturation and its application," *IEEE Trans. Autom. Sci. Eng.*, vol. 13, no. 2, pp. 868–875, Apr. 2016.
- [17] H. Pan and W. Sun, "Nonlinear output feedback finite-time control for vehicle active suspension systems," *IEEE Trans. Ind. Informat.*, vol. 15, no. 4, pp. 2073–2082, Apr. 2019.
- [18] B.-Z. Guo and F.-F. Jin, "Sliding mode and active disturbance rejection control to stabilization of one-dimensional anti-stable wave equations subject to disturbance in boundary input," *IEEE Trans. Autom. Control*, vol. 58, no. 5, pp. 1269–1274, May 2013.
- [19] D. Li, P. Ding, and Z. Gao, "Fractional active disturbance rejection control," *ISA Trans.*, vol. 62, pp. 109–119, May 2016.
- [20] S. Aole, I. Elamvazuthi, L. Waghmare, B. Patre, and F. Meriaudeau, "Improved active disturbance rejection control for trajectory tracking control of lower limb robotic rehabilitation exoskeleton," *Sensors*, vol. 20, no. 13, p. 3681, Jun. 2020.
- [21] C.-F. Chen, Z.-J. Du, L. He, J.-Q. Wang, D.-M. Wu, and W. Dong, "Active disturbance rejection with fast terminal sliding mode control for a lower limb exoskeleton in swing phase," *IEEE Access*, vol. 7, pp. 72343–72357, 2019.
- [22] D. Nadia, M. Bettayeb, and S. Djennoune, "Sliding mode active disturbance rejection control for uncertain nonlinear fractional-order systems," *Eur. J. Control*, vol. 57, no. 3, pp. 54–67, May 2020.
- [23] Y. Long, Z. Du, C. Chen, W. Wang, L. He, X. Mao, G. Xu, G. Zhao, X. Li, and W. Dong, "Development and analysis of an electrically actuated lower extremity assistive exoskeleton," *J. Bionic Eng.*, vol. 14, no. 2, pp. 272–283, Jun. 2017.
- [24] Y. Long, Z. J. Du, W. D. Wang, and W. Dong, "Human motion intent learning based adaptive motion assistance control for a wearable exoskeleton," *Robot. Comput.-Integr. Manuf.*, vol. 49, pp. 317–327, Feb. 2018.
- [25] Y. Long, Z. J. Du, W. D. Wang, and W. Dong, "Development of a wearable exoskeleton rehabilitation system based on hybrid control mode," *Int. J. Adv. Robot. Syst.*, vol. 13, no. 5, pp. 1–13, Oct. 2016.
- [26] Y. Long, Z. Du, L. Cong, W. Wang, Z. Zhang, and W. Dong, "Active disturbance rejection control based human gait tracking for lower extremity rehabilitation exoskeleton," *ISA Trans.*, vol. 67, pp. 389–397, Mar. 2017.
- [27] Y. Long, Z.-J. Du, W.-D. Wang, L. He, X.-W. Mao, and W. Dong, "Physical human-robot interaction estimation based control scheme for a hydraulically actuated exoskeleton designed for power amplification," *Frontiers Inform. Technol. Elect. Eng.*, vol. 19, no. 9, pp. 1076–1085, Sep. 2018.
- [28] Y. Long, Z.-J. Du, W.-D. Wang, G.-Y. Zhao, G.-Q. Xu, L. He, X.-W. Mao, and W. Dong, "PSO-SVM-based online locomotion mode identification for rehabilitation robotic exoskeletons," *Sensors*, vol. 16, no. 9, pp. 1408–1423, Sep. 2016.
- [29] L. Qiao and W. Zhang, "Trajectory tracking control of AUVs via adaptive fast nonsingular integral terminal sliding mode control," *IEEE Trans. Ind. Informat.*, vol. 16, no. 2, pp. 1248–1258, Feb. 2020.
- [30] L. Qiao and W. Zhang, "Adaptive non-singular integral terminal sliding mode tracking control for autonomous underwater vehicles," *IET Control Theory Appl.*, vol. 11, no. 8, pp. 1293–1306, May 2017.
- [31] Z. Chen, X. Yang, and X. Liu, "RBFNN-based nonsingular fast terminal sliding mode control for robotic manipulators including actuator dynamics," *Neurocomputing*, vol. 362, pp. 72–82, Oct. 2019.



**YI LONG** (Member, IEEE) was born in Bijie, Guizhou, China, in 1988. He received the B.S. degree in mechanical engineering from Sichuan University, Chengdu, China, in 2010, the M.S. degrees from the Harbin Institute of Technology, Harbin, China, in 2012 and 2017.

From July 2017 to May 2020, he worked as the Vice General Manager to lead a Robotics Team in Zhongshan, China. In August 2020, he joined Foshan Graduate School of Northeastern University, Foshan, China, as an Associate Professor. He has authored more than 20 academic articles and holds more than 50 patents. His current research interests include wearable exoskeletons, mobile robots, machine learning, and computer vision.



**YAJUN PENG** was born in Henan, China. He received the B.S. degree in mechanical engineering from the Harbin University of Commerce, Harbin, China, in 1998, and the M.S. degree from the South China University of Technology, Guangzhou, China, in 2012.

From July 1998 to October 2017, he worked as a Mechanical Engineer with an Automation Equipment Team. He is currently working as a Technical Manager with Zhongshan Walk-Best Intelligent Medical Device Company Ltd., Zhongshan, China. His current research interest includes the wearable exoskeleton.

...